Early Validation of the Multi-angle Imaging SpectroRadiometer (MISR) Radiometric Scale

Carol J. Bruegge, Nadine L. Chrien, Robert R. Ando, David J. Diner, *Associate Member, IEEE*, Wedad A. Abdou, Mark C. Helmlinger, Stuart H. Pilorz, and Kurtis J. Thome

Abstract—The Multi-angle Imaging SpectroRadiometer (MISR) instrument consists of nine cameras, four spectral bands each, and an on-board calibrator (OBC). Experiments using the latter allow camera radiometric coefficients to be updated bimonthly. Data products are thus calibrated to a stable radiometric scale, even in the presence of instrument response changes. The camera, band, and pixel-relative calibrations are accurately determined using the OBC. Conversely, as the OBC itself is subject to response degradation, MISR also conducts annual field vicarious calibration (VC) campaigns. The first of these, conducted June 2000 at a desert site in Nevada, has been used to establish the present absolute radiometric scale. Validation of this radiometric scale, using AirMISR, shows consistency to within 4%. Following these studies, however, it was determined that MISR radiometry is subject to scene-dependent effects due to ghosting that, for the Nevada test sites, reduces the apparent radiance by 3%. Correction for this effect is required in order to avoid radiometric errors over sites that do not exhibit the same background contrast. Additional studies are in progress, with plans to correct for scene-contrast effects in future Level 1B1 processing.

Index Terms—Calibration, Multi-angle Imaging SpectroRadiometer (MISR), radiometry.

I. INTRODUCTION

A. *The MISR Instrument*

THE Multi-angle Imaging SpectroRadiometer (MISR) [1] is one of five instruments on board the Earth Observing System (EOS) Terra spacecraft, and is one element of NASA's Earth Science Enterprise. MISR produces global data sets at nine-day intervals or less, depending on latitude. The effective center wavelengths, at 446, 558, 672, and 866 nm, have been computed using a moments (centroid) analysis within the region delimited by the 1% response points [2]. The effective bandwidths are 41, 27, 20, and 39 nm wide; these parameters are used to define an equivalent square-band response function for the sensor. Approximately 3% of the camera output comes from signals at wavelengths outside the 1% limits, for a spectrally neutral scene. Available data products include geo-located radiance images at nadir and off-nadir earth view angles. Each of the nine cameras has a unique name, and is associated with a specific view angle. The cameras view a target consecutively in the order Df (70.5° fore), Cf (60.0°), Bf (45.6°), Af (26.1°), An (nadir), Aa (26.1° aft), Ba (45.6°), Ca (60.0°), and Da (70.5°), with 7 min from first to last acquisition of a target. Here, the first letter of the camera name refers to the lens design and the second designates the fore-, nadir-, or aft-view directions with respect to the spacecraft track. MISR has 14-bit quantization, and therefore has roughly 16 384 gray levels (the finite video offset, and square-root encoding reduces this by about 300 counts).

MISR cameras acquire data in a pushbroom configuration, using the spacecraft motion to build up an image from each of the 36 charge-coupled device (CCD) linear arrays. The spatial resolution of the MISR cameras, established by the size of the detector elements, optical focal length, and spacecraft altitude, is 275 m cross-track (for the off-nadir cameras), or 250 m (for the nadir viewing camera). Downtrack instantaneous field-of-view increases due to the view angle effects, ranging from 214 m in the nadir to 707 m at the most oblique angle. Downtrack sampling is 275 m for all cameras. In practice, most data are acquired in Global Mode, where pixel averaging is performed in order to reduce the data rate. Here, 24 of the 36 data channels have been 4 × 4 pixel averaged before transmission from the instrument. For these channels data are transmitted at 1.1-km resolution. Even in Global Mode, however, high-resolution pixels are maintained for the four nadir channels, and the eight additional Band 3 (Red) channels. Complete high-resolution data sets for all 36 channels can be obtained from an instrument configuration called Local Mode. Here specific sites are targeted, such as those where intensive field campaigns are being conducted. The size of a Local Mode region is 300 km downtrack by 380 km crosstrack. About a dozen Local Mode sites are acquired routinely, including observations over desert calibration sites.

B. *MISR Data Products*

MISR data products include Level 1A (raw), Level 1B (radiance), Level 2 (science products), and Level 3 (global summary) data sets. The Level 1B1 data product is the focus of this paper. For this product, radiances are computed using an input data file called the In-flight Ancillary Radiometric Product (ARP). This file is updated following each MISR calibration experiment, and contains the radiometric coefficients needed to perform radiance scaling, that is conversion from instrument digital numbers (DN) to a measure of camera-incident radiance. MISR Level 1 radiances are not corrected to the "in-band" values, which is the radiance that would be measured if there were no out-of-band response. However, out-of-band response removal

is done prior to processing some Level 2 parameters, such as aerosol amounts. Level 1B1 radiances are reported at Global Mode resolution, i.e., at high resolution for 12 channels and at 1.1-km resolution for the remaining 24 channels. Where Local Mode targets are acquired, Level 1B1 data are also available at Local Mode resolution. Level 1B1 data are not resampled and do not achieve geolocation or channel coregistration.

Following creation of the L1B1 radiance product, the process flow continues with the Level 1B2 geolocated data product. Here, the data are resampled onto a Space Oblique Mercator grid, and in the process the 36 data channels are coregistered. These L1B2 data are used as input to the Level 2 science data production codes. Both the radiance and science products are constructed at the Atmospheric Sciences Data Center (ASDC), Langley Research Center (http://eosweb.larc.nasa.gov), and from there distributed to the scientific community. On the other hand, the ARP is constructed at the Jet Propulsion Laboratory (JPL), and delivered to ASDC for use in MISR data product processing.

C. Product Maturity Level

EOS data products are each classified as having obtained the Alpha, Beta, Provisional, or Validated level of product maturity. These descriptors, as defined by the Science Working Group for the AM Platform (SWAMP) meeting held October 30, 2001, are

1) *Alpha:* A test bed to discover and correct errors affecting the operability of the associated Product Generation Executive (PGE) at the Distributed Active Archive Center (DAAC). Data products are visible to the science team, but not the public.
2) *Beta:* Minimally validated. Early release to enable users to gain familiarity with data formats and parameters. May contain significant errors.
3) *Provisional:* Partially validated. Improvements are continuing. Useful for exploratory and process studies.
4) *Validated:* Uncertainties are well defined, and suitable for systematic, long-term studies.

As is expected, the uncertainties in MISR radiometric quality are better understood with time. To reflect this, MISR Level 1 data maturity was upgraded from Alpha to Beta on June 28, 2000. The key milestone achieved at this date was the demonstration of the in-flight calibration processing system. Both input and output variables were compared against predicted values. In addition, consistency of results during the initial three-month test period was evaluated. The Beta to Provisional status update took place on December 22, 2001. This upgrade followed the analysis of data acquired June 2000, the vicarious calibration campaign over Nevada desert playa, and the establishment of the present MISR radiometric scale. This study involved the validation of this scale via cross-comparisons among several sensor types. These early studies are reported in this document. More recent studies have been initiated on scene-dependent effects. Initial findings are briefly discussed at the end of this document. A reduction in contrast is observed, most probably the result of inter-reflections, or ghosting, between MISR-camera optical surfaces. Fortunately, it appears that a first-order correction for these is possible.

Work is in progress to better understand these effects, and to finalize a correction algorithm. The upgrade to Validated Product Maturity Level, per the definition developed by the EOS science community, is dependent more on understanding and documenting the errors in the data product, and does not preclude future algorithm improvements. For this reason the Validated upgrade took place April 16, 2002, and has preceded the implementation of a new Level 1B1 algorithm. Nevertheless, an improved L1B1 algorithm is anticipated for the future.

D. Calibration Overview

MISR camera specifications call for accurate absolute and relative radiometric calibrations. The absolute scale establishes a measure of the camera-incident radiance, in units of $W\ m^{-2}\ sr^{-1}\ \mu m^{-1}$. The relative calibrations minimize the uncertainty in the radiance reported for one camera relative to another camera, one band relative to another, or one pixel relative to another. It is intended that the calibration experiment be conducted using earth or flight targets that fill a cameras field-of-view. Likewise, the radiometric uncertainty reported for the MISR data products apply to scenes that are spatially uniform. Uncertainties are reported at the 1σ level of confidence, and are specified as a function of incident illumination level.

MISR makes use of an on-board calibrator (OBC) to provide temporal samplings of the radiometric response of each camera. The strength of the OBC is its ability to provide camera-, band-, and pixel-relative calibrations. OBC calibration experiments are conducted bimonthly (once every two months). It is desirable to deploy the calibration panels only as needed to capture camera response changes. The OBC consists of two Spectralon diffuse panels, and six sets of photodiode detectors. The latter measure solar-reflected light from the panels, and provide a measure of the camera-incident radiance. These are regressed against the camera output, in order to provide the radiometric response for each of the 1504 CCD detector elements per line array, nine cameras, and four spectral bands per camera.

As the OBC itself is subject to response changes with time, *in-situ* measurements of MISR incident radiances are also incorporated into the calibration program. These data are called vicarious calibration (VC) data. To acquire these data, a field-experiment is conducted in which surface reflectances and atmospheric properties are measured [3]. With these, top-of-atmosphere radiances are computed, and the calibration of the MISR primary OBC photodiode is adjusted to agree with this radiance value. For this purpose, an earth target that is homogeneous over three pixel widths ($\sim$750 m) is required, as well as clear-sky and low- aerosol conditions. When these criteria are met, extremely accurate radiance measurements can be made with these experiments. Data for a nadir view angle only are used, as the OBC is able to transfer this scale to the other camera angles, using simultaneous camera and photodiode views of the diffuse panel.

In addition to the OBC and VC experiments, the MISR team makes use of data from other sensors in order to validate the MISR radiometric scale. Validation experiments are used to assess the uncertainties in the calibration results; validation experiments are not used to adjust the radiometric response coefficients used to process MISR data. Moderate-Resolution

Imaging Spectroradiometer (MODIS), Landsat-7 Enhanced Thematic Mapper-plus (ETM+), and Airborne Visible/Infrared Imaging Spectrometer (AVIRIS), are examples of sensors used to provide a validation of the MISR nadir camera; AirMISR alone is able to validate the response of the MISR off-nadir camera calibrations. AirMISR is the airborne counterpart to MISR, but consists of a single camera gimbaled to the various MISR view-angle locations. This single-camera design allows an accurate validation of the MISR camera-relative response. Although the MISR radiometric scale could be adjusted using results from these cross-comparison studies, it is believed that a smaller radiometric uncertainty is achieved by using the OBC and VC experiments alone.

Within this document, other validation experiments will also be discussed. These include image-striping studies, used to validate the pixel-relative calibration, and a symmetry study that makes use of earth views. The latter is an additional technique that allows us to gain confidence in the MISR camera-relative calibrations. Neither of these experiments is used to establish the MISR radiometric scale, yet each is valuable in understanding the uncertainty of our results.

II. THE OBC CALIBRATION EXPERIMENT

A. On-Board Calibrator (OBC)

During the MISR design and build phase, precautions were taken to insure on-orbit radiometric stability [4]. For example, MISR utilizes ion assisted deposition (IAD) filters, which are physically dense and resistant to absorption of water or other contaminants. Both the cameras and calibration photodiodes have been manufactured using IAD technology, and thus are believed to be resistant to spectral shifts. In addition, camera sunshades and baffles minimize solar illumination onto the camera optical elements. Solarization of contaminants is one mechanism by which optical surfaces are thought to degrade in space [5]. Thus, these baffles help ensure the radiometric stability of the cameras. Preflight performance testing [2] has established the initial radiometric, and (assumed time-invariant) spectral and point-spread function responses. These tests demonstrated the quality of the MISR cameras, including high signal-to-noise (SNR), lack of polarization sensitivity, and lack of cross-channel interference.

Even with these precautions, radiometric response degradation of the cameras is anticipated and measured. With frequent updates to the response coefficients, the data products remain accurate even in the presence of sensor changes. To achieve this, once every two months MISR conducts an experiment using its OBC. The OBC measures light reflected from an extended, diffuse, reflectance standard, and thereafter infers the camera-incident radiance. Knowing this, and the camera output DN, a calibration is achieved. The OBC consists of six photodiode detector standards sets, including a goniometer, and two Spectralon diffuse panels [6]–[8]. One panel is deployed at the South Pole, and used to calibrate the fore- and nadir-viewing cameras; the other panel is deployed at the North Pole, and used to calibrate the aft- and nadir-viewing cameras. Each photodiode set is a compilation of four radiometric channels—one filtered to each of the four MISR spectral channels. One photodiode type

is termed "PIN" in reference to their p-i-n doped layer structure. The sets are named Da-PIN, Df-PIN, +y-PIN, −y PIN, and G-PIN, in reference to their location: "D" sets are coaligned with the D cameras, +y and −y sets are in reference to the spacecraft coordinate system with −y the sun-side of the spacecraft, and the "G" set is mounted to a goniometer which views the diffuse panel in the along-track plane. The final photodiode set is termed High Quantum Efficient (HQE) and is configured in a "trapped" orientation to provide 100% external quantum efficiency [9]. For the HQE devices, there are three photodiode detectors per channel to allow the light reflected from one diode surface to be collect by the next diode in the series. The blue-filtered HQE channel is used as the primary flight standard, selected for its on-orbit stability; transfer from this primary standard establishes the radiometric scale for all other photodiodes. The diversity of the OBC detector designs has proven useful in assessing the uncertainty of the in-flight calibration approach.

B. Early Mission Investigations

The MISR cameras saw first light on February 24, 2000, as the instrument cover was opened. The OBC hardware was exercised a few days later, as well as several more times that first month. Gain coefficient production, however, did not become operational until the April 27, 2000 experiment. Prior to this time validation studies were conducted on the input data streams and experiment design, including the panel deployment timing. One unanticipated investigation centered upon anomalous motor current transients observed during deployment of the South Pole calibration panel [10]. Concern for the motor was mitigated by moving the goniometer to +38° (aft view-angle position) prior to any further deployments of the South Pole calibration panel. It is believed that this procedure eliminated rubbing of the goniometer's aluminum shield against thermal blankets during panel movement, and thus removed the increased motor currents that were of concern. Routine bimonthly calibration observations were initiated after this investigation was closed and the appropriate operational procedures established.

C. Ancillary Radiometric Product (ARP)

The analysis of the OBC experiment data begins with an assumption that the instrument response can be modeled as

$$\mathrm{DN} - \mathrm{DN}_0 = G_0 + G_1 L_b + G_2 L_b^2 \qquad (1)$$

where

L_b spectral incident radiance, weighted over the sensor spectral response function and reported in units of [W m^{-2} sr^{-1} μm^{-1}];

DN   camera output digital number;

DN_0 DN offset, unique for each line of data, as determined by an average over the first eight "overclock" pixel elements (output samples which follow clocking of the CCD line array);

G_0 constrained to zero for the present algorithm;

G_1, G_2 response coefficients that provide the radiometric calibration of a specific pixel.

The G_1 and G_2 coefficients are re-computed for each experiment, whereas G_0 is constrained to zero, since the video offset

signal, DN_0, is within 1 DN of the dark current. It is noted that the G_2 coefficient is quite small, as the sensor is nearly linear except at very low radiance levels. Gain coefficients are computed for each of the 1504 active pixels per line array, in each of the nine cameras and four spectral bands. The reported radiances are band-weighted over the entire instrument spectral response function, specific to a given band. Although each of the 36 band and camera channels may be commanded to a unique integration time, altering this instrument configuration parameter is not foreseen, and the acquisition of calibration experiment data is conducted with the instrument remaining at its operational integration time settings. (These settings were determined preflight in order to balance signal-to-noise and dynamic range.) Once a calibration experiment is completed, coefficients are computed and packaged into an ARP file. This is sent to the ASDC within one week of data acquisition. Thus, the most recent values are used to process newly acquired sensor data.

The complete set of ARP parameters reside within one of four files [11], the Preflight Characterization, Preflight Calibration, In-flight Calibration, and Configuration Parameters files. Each file is written in Hierarchal Data Format (HDF). The gain coefficients, uncertainties, and signal-to-noise values reside in the In-flight Calibration file. These exist as a time series, updated after each OBC calibration experiment. The Preflight Characterization, Preflight Calibration, and Configuration Parameters files contain the instrument spectral response, exoatmospheric solar weighted irradiance values, and other parameters that are assumed to remain constant throughout the mission. For the remainder of this paper we will be referring only to In-flight ARP files.

Each coefficient set, and thus ARP file, is valid for the subsequent two months, until the next file is delivered. Together they form a series of files labeled T1 (preflight), T2 (first post-launch analysis, April 27, 2000), through Tx, where x is the time-series counter. More specifically, the ARP In-flight Calibration file name follows the format:

$$\text{MISR\_AM1\_ARP\_INFLTCAL\_Txxx\_Fyy\_zzzz.hdf} \quad (2)$$

where xxx is the time-series number, yy the file format identifier, and zzzz the revision number for a given time-series file. The abbreviation Tx_z is used in this paper to denote a specific in-flight, time-series file and revision number. Should MISR data be reprocessed in the future, the latest revision to each time-series file will be used. Prior to delivery of an updated data file, extensive testing is done using these new files. These testing files have the naming convention Txxx_SCFzzz. This nomenclature denotes that the file has been used only at the JPL Science Computing Facility (SCF), and has not been used in ASDC processing.

At this time, 14 ARP In-flight Calibration time-series files have been produced and delivered. The present in-flight calibration code has been in place since December 2001. Although the algorithm itself is believed to be well suited to meeting MISR calibration objectives, it is anticipated that changes in code input parameters will occur in the future. Specifically, once point-spread-function (PSF) and ghost-image corrections are made in Level 1B1 data products, MISR radiances will account for scene-dependent effects. To the degree that this changes the agreement with VC results, the photodiode calibration constants will correspondingly change, and new revisions to the ARP files will be required.

The remainder of this section covers the development of the present in-flight calibration algorithm. Changes have included moving from a linear to a quadratic calibration equation (see the linearity section, to follow), use of different detector standards, or different detector-standard calibration methodologies. To summarize [8], following extensive studies of the OBC, the use of the D-pin photodiodes has been adopted to calibrate all off-nadir cameras. As the diffuse panel is deployed to 67.5° with respect to the spacecraft, these two photodiodes view nearly along the panel normal (see figure in [8]). In this configuration, the panel reflectance is closer to the value of an ideal lambertian target, and errors in knowledge of the panel reflectance are minimized. Nevertheless, bidirectional reflectance factor (BRF) corrections are applied to the cameras not boresighted with the D-pin photodiodes. The earth-nadir viewing photodiodes view the panel at an extreme angle with respect to the panel normal. For this reason only the An camera is calibrated with an earth-nadir viewing photodiode. No BRF correction is required in this case, as the photodiode is coaligned with the camera under test.

Table I summarizes the updates that have led to the Provisional (current) OBC data processing algorithm. Each change resulted in an incremental reduction in the uncertainties of the resulting radiometric calibration coefficients. It is noted that the most significant change is the radiometric offset adjustment introduced on February 15, 2001. On this date a 9% increase in the radiometric scale of the primary flight photodiode standard (the HQE-Blue detector) was introduced, using June 2000 VC measured radiances as the standard. As this establishes the in-flight radiometric scale of the primary standard, it is applied retroactively, as new versions of previously delivered ARP files are created. As this scale is subsequently transferred to the remaining photodiodes, including those filtered to the green, red, and near-infrared wavelengths, the 9% adjustment applies to all spectral channels equally. The decision to make this scale change was based on knowledge that the OBC photodiodes response coefficient would need to be calibrated on-orbit. (Preflight testing was limited and failed to produce accurate calibrations. In addition, the response terms were expected to change and therefore an on-orbit determination was planned).

Because of changes in OBC data processing algorithms, future Level 1B1 scene-dependent radiometric corrections, and photodiode recalibrations, MISR data users should determine the heritage of the data products they use. To determine which ARP file was used to produce a Level 1B1 data product, one would use an HDF browser, such as hdfscan. (This software is scheduled to be available from the Langley DAAC, http://eosweb.larc.nasa.gov, and was written to view MISR data as well as generic HDF files.) Using such a data browser, one can read the metadata published within the MISR data product. The ARP file name can be found under Annotation Text: Input Data files. This file name can be compared to the latest delivered ARP file name, for a specific time period. ARP information can be found at the MISR site (see http://www-misr.jpl.nasa.gov; navigate to Calibration Results: ARP Summary). This web page

TABLE I
ARP ALGORITHM REVISION HISTORY

HQE-Blue: The blue-filtered HQE photodiode is used as the primary radiometric standard. This device is selected based upon its stability with time [8].	T2_4 August 24, 2000	Preliminary scale, in that the on-orbit absolute calibration had not yet been established.
VC scaling: The June 11, 2000 vicarious calibration experiment is used to calibrate the HQE-Blue photodiode standard.	T2_5 February 15, 2001	9% increase in MISR radiometric scale, for all channels. The uncertainty in MISR-reported radiance is reduced from 10% to 4% for the Nevada desert scenes.
Quadratic: A quadratic calibration equation is introduced, shown to improve the radiances reported over dark targets, such as oceans (see latter section).	T8_1 May 17, 2001	Reduces the residuals in the calibration equation fit. Changes in MISR reported radiances are negligible for equivalent reflectances >0.02, and a few percent otherwise.
Provisional: The South Pole calibration panel is shown to have measured bi-directional reflectance function (BRF) data that agree with the preflight determination. The bi-monthly transfer of radiometric response from the (stable) HQE-Blue device to the remaining (less stable) devices is done using data from the South Panel views. The goniometer is used to update the BRF profile for the North calibration panel [8].	T12_1 December 22, 2001	Aft-camera radiances decreased by a few percent. Improves the camera-relative calibration from 4% uncertainty to a 2% uncertainty.

contains OBC calibration experiment dates, lists all algorithm changes, and gives coefficient summary reports for a typical on-axis pixel, per channel.

D. MISR Trend Analyses

The OBC data processing code, referred to in the above section, can be broken down into the modules discussed as follows.

1) *Data Input:* Solar ephemeris data, panel-deploy flag, high rate photodiode and camera data are collected as processing inputs.
2) *OBC Data Preprocessing:* Observations where the photodiode current is less than 0.8 nA are excluded, due to concerns of nonlinearity in this region. Next, the OBC data are interpolated from 208 msec repeat time of the diode measurements to the CCD 40.8-msec line-repeat time. Panel BRF differences between the photodiode and camera view angles are accounted for using the preflight BRF measurements [12], reporting radiances as they would have been measured in the camera view direction.
3) *Regression:* A least-squares fit of the photodiode radiances to camera output DN is performed, using (1) to extract the G response coefficients.
4) *Signal-to-Noise (SNR):* The measured signal-to-noise is computed from the mean and standard deviation ratio, over a 100 pixel boxcar which slides over each pixel. An average for each of the 36 channels is reported to the ARP file. Other detector health metrics include the Detector Data Quality Index (DDQI), discussed in Section IV.

Output from the code is used to produce the ARP file that results from a given experiment. One way to summarize the results from each calibration experiment is to use the gain coefficients to compute the incident radiance needed for a DN output of 10 000 counts. Response coefficients for a typical pixel, se-
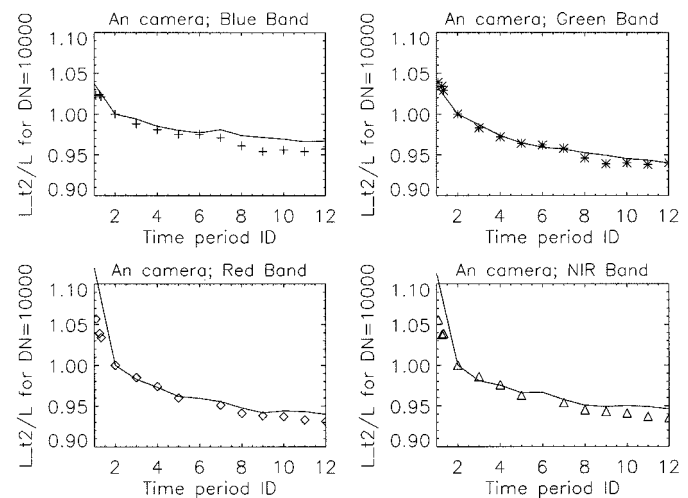
Fig. 1. An-camera degradation with time, normalized to April 27, 2000. Solid lines: computed from ARP gain coefficients. Symbols: computed from DN/irradiance for diffuse panel views. The latter analysis reports additional early-mission points, for times when ARP processing was not available.

lected from the on-axis portion of each array, are used. This resulting radiance value is normalized, and the inverse taken so that degradation may be demonstrated. This output represents the instrument degradation with time, and is plotted with solid lines (Fig. 1). (Degradation is defined here as the decrease in DN output with time, for a fixed incident radiance. From (1), this degradation can also be expressed as the decrease in the inverse of incident radiance needed to achieve a fixed DN output.) In this study, the April 27, 2000 date was used to normalize the data, as this is the first in-flight experiment data for which ARP coefficients were produced. It is shown that a 5% degradation from cover open to April 27, 2000, occurred (a two month period); such a rapid early mission degradation was expected, and

is typically of on-orbit sensor response changes. The present response change is roughly 2% per year (1.5, 2.0, 2.5, and 2.4% respectively for the four bands).

An independent method to express instrument degradation is shown by the symbols in Fig. 1. These data have not been generated from ARP gain coefficients, but rather instrument DN output (with the video bias signal removed) while viewing the deployed calibration panels. As the diffuse panels are known to be optically stable on-orbit [8], any change in DN can be attributed to camera response degradation. Data for the Red and Near-Infrared (NIR) channels are missing for several dates, due to a moratorium on South Pole panel deployment. (The An camera uses the North Pole panel to calibrate the Blue and Green channels and the South Panel for the Red and NIR channels. It is not possible to collect high resolution data in all four An bands simultaneously, due to instrument data rate limitations.) The raw DN output values have been multiplied by R^2/μ_0, the earth–sun distance squared divided by the cosine of the solar zenith angle onto the panel. This correction removes the first-order sensitivity to solar illumination differences from one observation to the next. These data have also been normalized to the value reported for first calibration experiment, April 27, 2000. Time T1 is the preflight calibration, T2 the first in-flight calibration (April 27, 2000), and T12 corresponds to December 14, 2001. The figure shows the instrument response to be 2–6% lower, depending on spectral band, on April 27th, as compared to the initial cover-open response. Both analyzes show the rate of instrument response change to have decreased with time.

III. IN-FLIGHT CALIBRATION PROCEDURES

A. Absolute Calibration via Vicarious Calibration (VC)

Instrument specifications call for the MISR absolute radiometric scale to be established to within 3% uncertainty, for an extended uniform bright target. As stated above, MISR makes use of annual VC data to maintain this scale throughout the mission by correcting for on-orbit degradation of the OBC primary photodiode standard. The HQE-Blue photodiode was selected as the standard due to its on-orbit stability. The June 11, 2000 VC provided the first on-orbit absolute calibration of this photodiode, and that of the instrument. The VC experiment was repeated June 30, 2001, with consistent findings. One recently discovered limitation of this study, however, is that no scene-contrast adjustment to the MISR data was applied, prior to setting the radiometric scale. The Nevada desert playas, used in these VC experiments, are 1.5–2.0 times brighter than the surrounding land area. The magnitude of scene-contrast effects, for this site, is estimated to be 3%. A preferred approach would be to apply a contrast-correction algorithm, based upon the sensor-measured within-field illumination, prior to setting the radiometric scale. This will be implemented in the next phase of our Level 1B software. Until then MISR data may be calibrated 3% too high over extensive uniform areas such as the Sahara desert, which fill the field-of-view of the MISR cameras. Radiometric errors for less uniform scenes need to be evaluated, both with and without a contrast-enhancement correction. With this exception, the VC and OBC procedures developed to date, and reported here, are well suited for future MISR calibrations.

Fig. 2.   (Left) Lunar Lake and (right) Railroad Valley targets, Nevada, as acquired by MISR on June 11, 2000. Area shown is approximately 84 × 84 km^2. Symbols identify latitude, longitude locations listed in Table II.

TABLE II
VICARIOUS CALIBRATION TARGETS

Target	Latitude/ Longitude, degrees	Extent of playa region, km^2	Red band uniformity (equivalent reflectance)
Lunar Lake, Nevada	Bright pixel: 115.991 West x 38.398 North	1.1 x 1.1	1.0% (0.43)
Railroad Valley, Nevada	VC site: 115.6712 West x 38.4956 North	8.8 km NS x 8.7 km WE	1.8% (0.34). Uniformity is 0.7% over 275 m scales.

The preferred MISR vicarious calibration approach is to make use of simultaneous field, aircraft, and on-orbit sensor data. The aircraft counterpart to MISR, AirMISR, is an ER-2-based sensor with 7-m resolution in the nadir at 20-km altitude, and creates images 10 km wide × 9 km long [13]. (The AirMISR georectified data product used here is averaged to 27.5-m resolution.) AirMISR enables validation of the MISR camera-relative calibration, as its single camera is deployed to each of the nine MISR view angles in turn. In addition, data from the PARABOLA instrument [14] measures the playa bidirectional reflectance factor (BRF). MISR, AirMISR, and PARABOLA data sets have been acquired for each of the two VC experiments conducted to date.

The brightness and uniformity of two commonly used VC playas, shown in Fig. 2, are presented in Table II. Desert playas within the western United States are preferred, based upon their optical properties, predictably sunny conditions, and low atmospheric aerosol loading. Railroad Valley is located some 12 km northeast of the Lunar Lake Playa. Although regions of Lunar Lake are brighter and more uniform than Railroad Valley, the

latter is preferred for moderate spatial resolution sensors, such as MISR. Lunar Lake has the harder surface, and ground tracks remaining after field studies are less pronounced than at Railroad Valley. AirMISR acquired data sets over Lunar Lake in June of 2000, and over both Lunar Lake and Railroad Valley in June 2001. MISR, having a 380-km swath width, acquired data simultaneously over both targets on both dates. Presented here is the validation of the VC radiance scale. Reference [3] gives details of this VC experiment.

Flight and aircraft sensors involved in the June 11, 2000 experiment were the MODIS, Landsat-7 Enhanced Thematic Mapper-plus (ETM+), IKONOS, AirMISR, and AVIRIS. Field teams were available from the Jet Propulsion Laboratory for this experiment, as well as from the University of Arizona, Optical Sciences Center.

The MISR data were acquired on Orbit 2569, Path 40, Block 60, at 18:50 UT, 11:50 Pacific Daylight Time (local time). The data acquisition time is for the initial acquisition, the Df camera. Seven minutes are required for all nine cameras to complete the scene acquisition. The Terra track was 190.4° in azimuth from North. AirMISR had three successful acquisitions of this region. In Runs 2 and 5, the aircraft had a south to north track; for Run 3 the aircraft moved from North to South, coincident with the Terra overpass. The multiple runs were acquired in order to lower the risk of data loss due to data acquisition timing errors. The data presented here are from Run 3, that coincided with Terra.

The computed VC top-of-atmosphere radiance [3] showed initial MISR radiances, established using the initial on-orbit calibration of the HQE-Blue standard, to be low by a factor of 0.91. The uncertainty for this type of VC experiment is small: the desert playas are uniform, sky conditions clear, and the appropriate measurements made at the time of overflight. It is also known that the preflight calibration of the OBC photodiodes is uncertain, due their documented uncertainty with respect to panel-predicted radiances [8]. Subsequently, the response coefficient for the HQE-Blue flight standard has been adjusted to agree with the VC data. This standard scale change propagates to a change in ARP coefficients, and thus to the MISR radiance data products. The desired outcome is to have coefficients which, when used to process MISR data over Lunar Lake on this date, would produce Blue Band radiances equal to the VC radiances.

A summary of the uncertainties for the VC computed radiances, and MISR cameras, are provided in Tables III and IV. At the MISR spatial scales the uncertainties are 4% for the Nevada targets, and 7% otherwise.

1) Absolute Response Validation Studies Using Cross-Sensor Data: Figs. 3 and 4 present the validation of the present MISR in-flight radiometric scale at the Nevada sites. Shown are the radiances from reprocessed MISR images (using T3_SCF10 which has the 9% scale adjustment, Provisional ARP algorithm), AirMISR (AirMISR ARP T1), MODIS (V3, Bands 3, 4, 1, and 2, 500-m data), and the VC computations. All data sets were acquired on June 11, 2000.

Fig. 3 presents the comparison between MISR, AirMISR, Landsat, MODIS, and VC data over Lunar Lake. In order to compare data sets at comparable resolutions, AirMISR Level

TABLE III
VC RADIANCE COMPUTATION, BLUE BAND

Error source	Abs. Unc., %
Solar irradiance knowledge	2
Spectralon reflectance knowledge	1.5
Surface reflectance, including errors in geolocation, in-situ sampling, and inhomogeneity	1
Relative surface BRF knowledge	1
Atmosphere characterization	1
Cosine of solar zenith	< 0.1
Field instrument SNR	0.1
MISR camera SNR	0.1
Earth-Sun distance	negligible
Root-sum-squares	3

TABLE IV
MISR ABSOLUTE CALIBRATION UNCERTAINTY, VC-BASED APPROACH

Error source	Abs. unc., %	Notes
VC radiance	3	From Table 3.
VC to Blue-HQE transfer	2	
Blue-HQE temporal stability	1	One-year time scale, equivalent to VC repeat cycle.
Camera to photodiode view angle BRF ratio	1	
Blue-HQE to operational photodiodes	0.5	Spectral uncertainty of Spectralon on-orbit. Timing errors
Diffuse panel spatial uniformity	0.5	
Diode SNR	0.1	
Calibration equation functional forms	0.1	Negligible in the 0.05-1. equivalent reflectance range. May be as large as 5% for reflectances <0.02.
Out-of-band response	negligible	Level 1B1 data products report total-band weighted incident radiances.
Root-sum-square	4	Radiance error for Nevada desert sites.
Scene dependent effects	3	Additive error will affect radiometry over uniform scenes, on MISR swath scale.
Total uncertainty	7	Present uncertainty for extended scenes, such as Sahara desert sites.*

- Scene-dependent effects are uncorrected at this time, yielding a 7% radiometric uncertainty in radiances reported over uniform scenes, on camera field-of-view scales. Future L1B1 corrections for this effect will reduce the radiometric uncertainty to within 4%, irrespective of the background.

1B2 samples were averaged 10 × 10 pixels, transforming the 27.5-m pixels into 275-m pixels, equal to MISR L1B2 nadir resolution. Use of a radiative transfer code allowed AirMISR data to be scaled from 20-km to top-of-atmosphere. The derived scale factors are 1.01, 0.98, 0.99, and 1.0, a correction ≤2% in all bands. The 30-m Landsat data were average over 9 × 9 pixels, in order to provide radiance averages over MISR pixel dimensions. In using Landsat data, correction factors of 0.914,
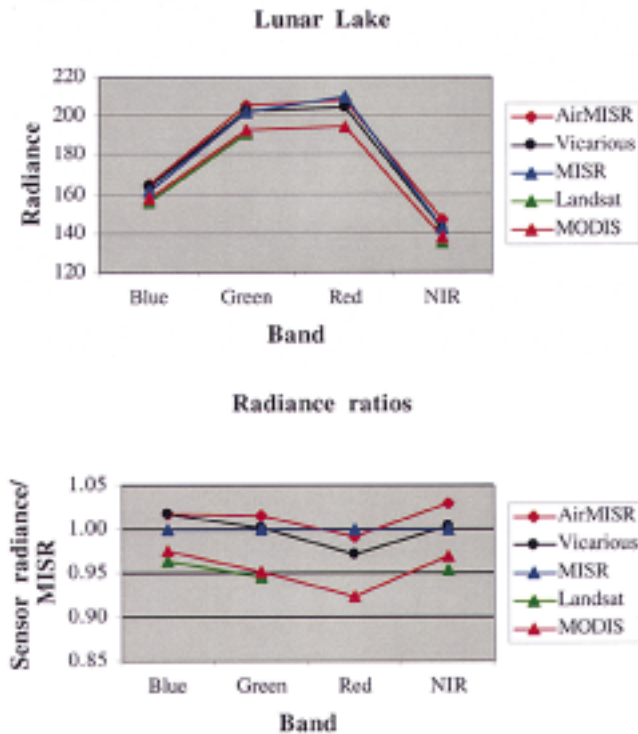
Fig. 3. Lunar Lake radiance comparison study, June 11, 2000, 115.991 W latitude, 38.398 N longitude. MISR An camera, T3_SCF10, MODIS V3 data. Top: radiances [W m^{-2} sr^{-1} μm^{-1}]. Bottom: sensor/MISR radiance ratios. Data corrected to MISR orbit time, altitude, and bandpasses.

Fig. 4. Railroad Valley radiance comparison study, June 11, 2000, 115.6712 W latitude, 38.4956 N longitude. MISR An camera, T3_SCF10, MODIS V3 data. Top: radiances [W m^{-2} sr^{-1} mm^{-1}]. Bottom: sensor/MISR radiance ratios. AirMISR data were not acquired over Railroad Valley on this date.

0.996, 0.996, and 0.923 were applied, to account for spectral response function differences. An additional correction factor of 1.042 was applied to the Landsat data, as the Landsat overpass was 40 min prior to Terra. This latter factor accounts for the difference in solar illumination angle at the overpass time (20.1° for Terra; 25.7° for Landsat).

The spectral response scale factors for MODIS Vegetation Band 3 (Blue), 4 (Green), 1 (Red), and 2 (NIR) are 0.906, 1.002, 0.986, and 0.982, respectively. No cosine timing adjustments are needed when comparing MODIS to MISR. MODIS 500-m data are at coarser resolution than the other data sets—hence geolocation errors and playa homogeneity increase the error associated with this comparison. As shown in Fig. 3(b) the VC radiances, AirMISR data, and the MISR radiance images all agree to within 4%.

Fig. 4 compares MISR, Landsat, and MODIS radiances over Railroad Valley. As this site is larger in extent, geolocation and surface homogeneity are smaller error contributors to the comparison, as compared to the Lunar Lake site. Differences between MODIS and MISR, following MODIS scaling to the MISR response functions, are 0, 4, 7, and 2%, respectively, for MODIS Bands 3, 4, 1, and 2. The Landsat sensor underwent a gain change between Railroad Valley and Lunar Lake on this date. It is for this reason that the Landsat Band 3 data are saturated over Lunar Lake, to the south, but not over Railroad Valley.

2) Spectral Response Comparisons: From the above analysis, a correction for differences in spectral response functions

need to be made when comparing MISR to Landsat or MODIS radiance values. For the L1B data products, MISR reports radiances weighted by the total-band response; MODIS and Landsat report radiances at in-band wavelengths. To compare these data, sensor spectral response functions are plotted in Fig. 5. Using these data, the spectral response and solar-irradiance weighted effective center wavelength, and bandwidth are computed, using a moments (centroid) analysis [2]. For Landsat and MODIS, the in-band response functions were utilized; for MISR, data were considered within the region delimited by the 1% response points. These parameters are listed in Table V for the various sensors. The parameters may differ from those published elsewhere since a solar-weighted moments analysis has been used here. These center wavelength and bandpass parameters are not used in the algorithm to convert cross-sensor radiances into effective MISR-measured radiances, for view of the same scene. They are used only as instrument descriptors, independent of scene features.

To correct the radiance data for spectral response differences, the following integrals are computed

$$\frac{L^{misr}}{L^{sensor}} = \frac{\left(\int \rho_\lambda E_{0\lambda} R_\lambda^{misr} \, d\lambda\right) / \left(\int R_\lambda^{misr} \, d\lambda\right)}{\left(\int \rho_\lambda E_{0\lambda} R_\lambda^{sensor} \, d\lambda\right) / \left(\int R_\lambda^{sensor} \, d\lambda\right)}. \quad (3)$$

Here, $E_{0\lambda}$ is the exoatmospheric solar irradiance, and ρ_λ is the top-of-atmosphere (TOA) spectral reflectance. These scale factors are shown in the last two columns of Table V for a two scene types. The first is representative of desert playas. During the
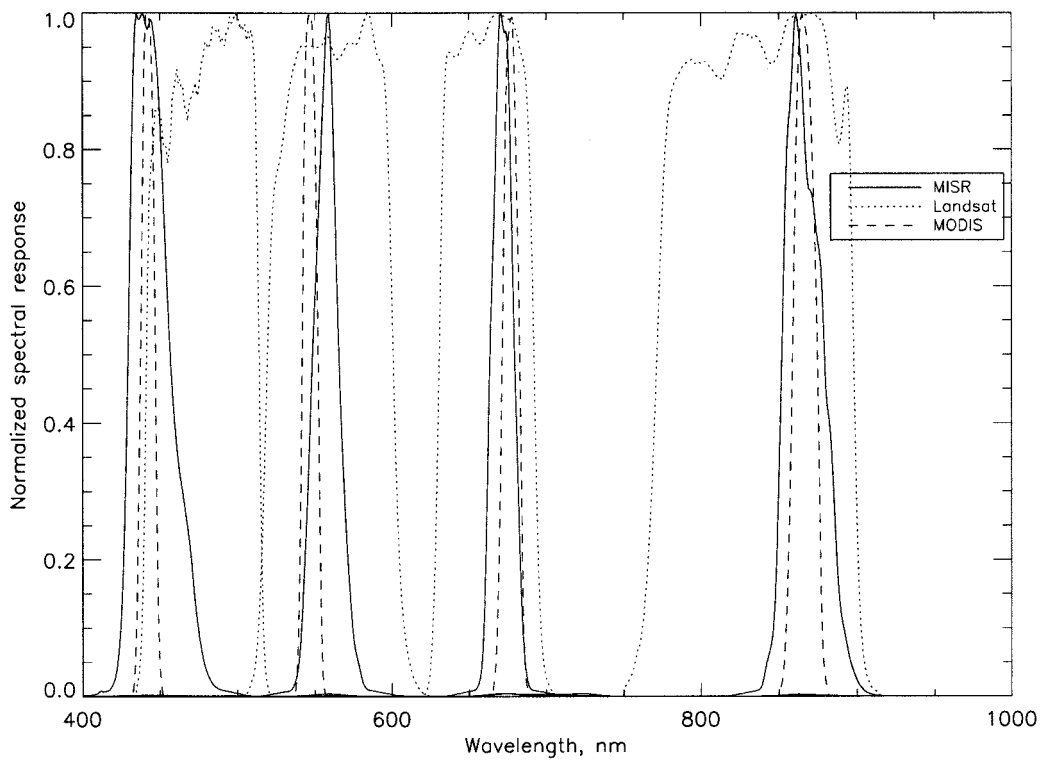
Fig. 5. Comparison of MISR, Landsat, and MODIS land (bands 3, 4, 1, and 2) spectral response functions.

TABLE V
COMPARISON OF MISR, AIRMISR, LANDSAT, AND MODIS SPECTRAL RESPONSE PARAMETERS

MISR Band no.	Sensor	λ_c, nm	$d\lambda$, nm	$E_{0,b}$ [W m^{-2} mm^{-1}]	Sensor/ MISR radiance scale factor* Desert	Ocean
1	MISR	446	41	1871	1	1
2		558	27	1851		
3		672	20	1525		
4		866	39	969		
1	AirMISR	447	44	1868	1.002	1.001
2		559	29	1850	0.998	1.004
3		672	21	1527	1.005	0.973
4		867	39	970	1.000	0.998
1	Landsat	478	73	1966	0.914	1.122
2		561	83	1841	0.996	0.984
3		661	63	1552	0.996	0.959
4		832	129	1054	0.923	0.905
1	MODIS Band 3	466	21	2015	0.906	1.054
2	MODIS Band 4	554	21	1858	1.002	0.978
3	MODIS Band 1	646	50	1601	0.986	0.903
4	MODIS Band 2	856	45	989.8	0.982	0.997
1	MODIS Band 9	442	11	1865	1.010	0.978
2	MODIS Band 12	547	12	1870	1.012	0.933
3	MODIS Band 14	677	14	1505	1.003	1.027
4	MODIS Band 16	866	19	969.7	1.005	1.029

* Values shown are spectral response correction factors for a desert and an ocean scene. Lunar Lake top-of-atmosphere spectral radiances, as computed for the June 2000 VC campaign, were used to simulate differences for desert-type scenes. The top-of-atmosphere ocean spectral radiances were computed using MISR measurements over the Moby buoy, off the coast of Lanai, Hawaii.

2000 VC campaign at Lunar Lake, spectral surfaces reflectances were measured, as well as spectral optical depth parameters. Using a radiative transfer code, the top-of-atmosphere functions are computed [3], and used in (3). The second type modeled was an ocean scene, as represented by the Moby Buoy site in Hawaii. Here, MISR top-of-atmosphere radiances were used to define values at MISR wavelengths, and linear interpolation was used to approximate radiances at other wavelength values. The range

TABLE VI
CAMERA-RELATIVE UNCERTAINTY, OBC-BASED SCHEME

Error source	Rel. unc., %	Note
Camera to photodiode view angle BRF ratio	1	
Blue-HQE to operational photodiodes	0.5	Timing errors. Goniometer transfer to D-PIN photodiodes.
Diffuse panel spatial uniformity	0.5	
Diode SNR	0.1	
Root-sum-square	1.2	

Fig. 6. Comparison of MISR 275-m data to AirMISR (10×10 averaged) radiances [W m^{-2} sr^{-1} μm^{-1}], red band.

in these scale factors demonstrates considerable scene dependence. It is noted, by inspection of (3), that the absolute magnitude of the scene reflectance does not contribute to these scale factors. Thus, assuming Railroad Valley and Lunar Lake sites to have the same relative TOA reflectance function, the scale factor for one is representative of that for the other site. The more similar the passbands are from one sensor to another, the less the scale factors depend on scene type.

B. Camera-Relative Calibration Using the OBC

The specification for camera-relative calibration calls for the radiance of one camera to be within 1% (1σ) as compared to another camera of the same spectral band. The OBC provides the camera-relative calibrations. During each OBC experiment, five cameras see a particular diffuse panel simultaneously at one pole, five at the other pole, with the nadir camera viewing both panels. The largest uncertainty in this approach is knowledge of the calibration panel BRF correction factor, from the photodiode view to camera view. The on-board goniometer has been useful in showing that the BRF values of the two panels are different. The BRF of the South calibration panel matches the database acquired preflight; the BRF of the North calibration panel differed, by a few percent, from that measured preflight and has now been updated with the flight data. The error sources for the camera-relative approach are shown in Table VI.

One alternative would be to use the VC radiances for all cameras. This is undesirable, however, in that VC uncertainties increase with off-nadir viewing angles. This is due both to uncertainties in aerosol parameter knowledge, as well as increases in surface inhomogeneity. The latter is due to the increase in sensor instantaneous fields-of-view with view angle.

1) Camera-Relative Validation Using AirMISR: The OBC is used to establish the MISR camera-relative radiances, however an independent technique is desirable to validate this scale. AirMISR is the primary tool used in this validation process. AirMISR views a given target coincident with a MISR overpass. The principal difference between the two instruments is that AirMISR data are obtained from a single camera, and therefore have no camera-relative errors with view angle (no scan-angle effects have been identified). The AirMISR and MISR radiances measured over Lunar Lake are shown in Fig. 6, for Band 3 (Red) data at 275-m resolution. (The other MISR bands are at lower resolution, for the L1B2 data used here, and difficult to use on this small desert playa.) The AirMISR data have been 10×10
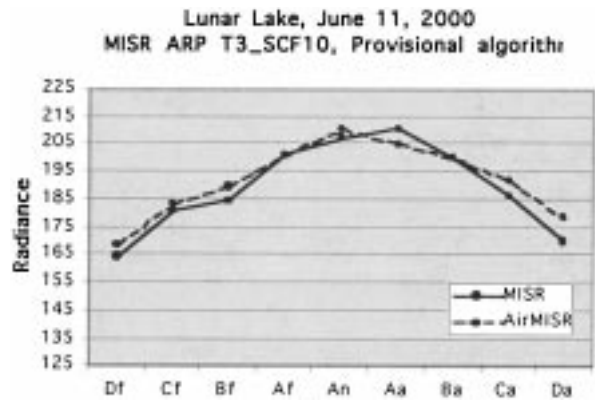
pixel degraded, to yield data at 275-m resolution. The comparison has been done at the playa center, over a bright region that is easy to identify from one image to the next. Uncertainties in this method are due to relative geo-location errors, and offset uncertainty for the AirMISR pixel-averaging process. Scene-dependent effects are thought to be small, in terms of camera-relative errors. These data verify that MISR camera-relative calibrations are known to the 1–2% level. These results are much improved over algorithms that were used prior to making use of the flight goniometer to measure the panel BRF, which showed 4% uncertainties. Thus, AirMISR data have established that the goniometer-measured panel reflectances are indeed correct.

2) Camera-Relative Validation Using Symmetrical View Angles: An independent method of verifying camera-relative radiometric errors involves the analysis of earth view data, at locations where the view azimuth angles are symmetrically placed relative to the solar azimuth direction. In order to identify scenes in which the fore- and aft-view angles were symmetrical with respect to the principal illumination plane, use was made of parameters in the L2AS Aerosol product. This product contains view zenith and relative view-solar azimuth angle for all nine cameras, and equivalent reflectance averaged over 17.6×17.6 km^2 regions. Subregions, 1.1 km in extent, that violate angular smoothness and correlation tests are filtered from these averages. Only land data are used because over land the same set of subregions is used for all cameras. In order to guard against heavy cloud contamination and parallax effects, at least 200 out of the possible 256 subregions had to survive smoothness and angular correlation screens. Locations where the relative view-solar azimuth angles were within 1° of each other for symmetric fore/aft camera pairs were identified. If the blue band equivalent reflectance of the forward camera exceeded 0.25, the data were not used as an additional screen against clouds. Unless there is some preferential orientation of the land terrain features, equivalent reflectances from a fore/aft pair at symmetric relative azimuth angles are expected to be statistically identical under the established conditions. It is assumed that any preferential surface features orientation is random, and thus contributes to statistical noise but not to a bias. Since symmetric fore/aft relative azimuths occur near the solar equator, land data over Africa were chosen for this study. Depending on which orbits
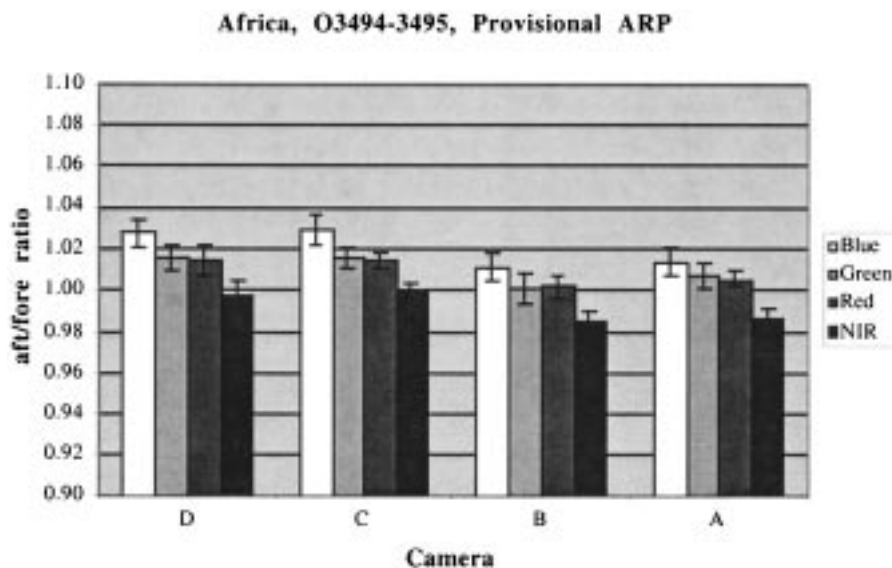
Fig. 7.   Fore–aft camera ratios for current (Provisional) ARP processing algorithms.

are used in the analysis, the aft-to-fore ratios vary by a few percent. Nevertheless, this technique validates the aft/fore camera relative response to within this uncertainty. The results are presented in Fig. 7 where slightly higher radiances are reported for the aft cameras. As a worst case, a ratio of 1.03 is shown for the D-camera blue band, with unity the desired result.

C. Band-Relative Calibration

Specifications on the MISR band-relative calibration call for an uncertainty of 1% (1σ). This is best achieved using views of the OBC diffuse panel. Green, Red, and NIR secondary photodiode standards are first calibrated against the HQE-Blue photodiode assuming the currents are proportional to the photodiode responsivity [8]. The response of the photodiode to be calibrated is adjusted, for each OBC experiment, such that its ratio with the HQE-Blue response agrees with their respective current ratios. This step allows drift in any of the secondary photodiode standards to be accounted for, relative to the primary standard. This approach is dependent on knowledge of the relative spectral reflectance properties of the flight diffuse panels. It is believed, based upon preflight testing, that this is constant to within 1–2% [15]. The uncertainties in the approach are given in Table VII.

It is noted that in this approach the VC data are not used to scale all MISR spectral channels. Band-relative error sources for this VC approach would include the uncertainty in the exoatmospheric solar irradiance. In comparing the World Radiation Center solar spectrum, [16], to that published by Thullier, [17], a 0.5% difference is noted in the mid-visible, however there exists a 4% discrepancy in the Near Infrared. Thus, considerable band-dependent errors are noted. In addition, Rayleigh and aerosol scattering have strong wavelength dependencies, hence the uncertainties due to these sources are likewise wavelength dependent.

D. Pixel Relative Calibration

MISR specifications call for the pixel-relative calibration to be performed to within 0.5% (1σ) uncertainty. We believe this

TABLE VII
BAND-RELATIVE UNCERTAINTY, OBC-BASED SCHEME

Error source	Rel. unc., %	Notes
Secondary standard calibration, relative to the HQE-Blue.	1	Spectralon spectral uniformity. Timing errors. Knowledge of detector area-field-of-view (AΩ) relative error.
Photodiode to camera transfer	1	Relative BRF errors.
Diffuse panel spatial uniformity	0.5	
Diode SNR	0.1	
Root-sum-square	1.5	

specification is met, since the Spectralon uniformity is good to within this amount. During OBC experiments there appears to be no abrupt changes in panel illumination, or spatial differences in the panel illumination. These would increase the pixel-relative calibration errors. It is noted, however, that a uniform stray light field cannot be ruled out. Such might be present due to earthshine onto the panel, or reflections from MISR radiators onto the panels. Such uniform stray-light fields would not increase the pixel-relative uncertainty. One test of this calibration is the lack of striping in the data product, to within 0.5% radiometrically.

As an example, vertical banding was observed in early MISR data, prior to the first in-flight update of the radiometric coefficients. Fringing patterns, with 2% peak-to-peak amplitude, were observed; these effects are reduced below 0.5% with use of the OBC bimonthly results. The de-striping is termed "flat-fielding" and is the effect of removing camera field-of-view response differences, using views of the Spectralon diffuses panels. This would be a difficult task to accomplish using earth scenes, due to spatial inhomogeneity and varying atmospheric transmittance and bidirectional reflectance across the 380-km swath. Thus, we believe the band-relative calibrations can best be achieved by using the OBC, rather than other methodologies.

IV. INSTRUMENT PERFORMANCE STUDIES

A. Ghost Images

As a validation of the radiometric scale over different sites, ratios of MODIS to MISR were calculated. The results were surprising, in that scene-dependent differences were shown, as demonstrated by Table VIII. The results are not due to sensor spectral response differences, since the magnitude of the effect is greater than the uncertainty in the spectral response correction factors. Railroad Valley was used as the Nevada site (July 16, 2001), with target to swath-average radiance ratios of 1.6, 2.0, 2.0, and 1.5 in the four bands. By comparison, the Sahara site (Libya, July 22, 2001, 13.35 E, 24.42 N) has target radiances much closer to the swath average. From this table we see a difference in MODIS to MISR ratios of 0.03, 0.03, 0.04, and 0.03 respectively for the four bands. The cause of this contrast-reduction has recently been investigated, and will be reported in detail in a separate publication. These studies have shown that the MISR camera designs are subject to low-level ghost-image effects. This is demonstrated both by laboratory testing of the MISR engineering-model camera, and through ray tracing using the lens design model. The latter shows that light rays can be back reflected at each optical interface, and again redirected to allow a secondary image to be recorded. Many such surfaces are involved in this process, thus many secondary images are formed, mostly out-of-focus. The result is that light from a bright portion of the scene is reflected into darker portions of the image. For the bright Nevada target, however, the effect reduces the measured radiances, as more light is lost in this process than added back from other target locations. Thus, the process has the effect of reducing scene contrast. Ghost-image effects are not observed in uniform scenes where there is no contrast.

In the near future, MISR plans to construct an algorithm to perform ghost-image corrections to the radiance products. Once implemented, radiances reported over the calibration sites in Nevada will be forced to remain unchanged, since they are defined by the VC ground-truth experiments. Any brightening due to ghost image corrections will be intentionally compensated by a reduction in that radiometric scale established by the gain coefficients. For all other scenes the radiance will differ as compared to the values reported currently. For the Sahara scenes, there is nearly no ghost-image correction. Thus, as the gain coefficients will be adjusted to decrease the radiometric scale, the radiances reported for these uniform scenes will decrease. The magnitude of this effect is estimated to be about 3% at this time.

Validation of the ghost-correction algorithm will require scene-independent radiance ratios for MISR as compared to another reference sensor. MODIS is thought to be a good reference for this application, since it is a scanner. MISR, being a pushbroom instrument, views the entire swath simultaneously, thus some degree of optical cross talk is inevitable.

B. Vignetting

The coefficients in the ARP files for the Aa and Af cameras are drastically different for the edge regions. Portions of these cameras are partially vignetted by an instrument baffle plate. The flat-field response of the Af camera shows there is a 60% response drop at the edge of the field. The vignetting begins about 75 pixels from the CCD array edges, and thus affects about 10%

TABLE VIII
SCENE-DEPENDENT RADIANCE RATIOS

Target	MISR Band	Site radiance	CCD line average	MODIS/ MISR radiance
Nevada	Blue	141.4	87.0	1.01
	Green	172.3	87.8	0.98
	Red	166.5	83.9	0.96
	NIR	113.3	74.2	0.97
Sahara	Blue	113.1	105.2	0.98
	Green	170.3	146.7	0.95
	Red	243.0	211.7	0.92
	NIR	181.9	159.0	0.94

of the detector elements in these two cameras. The in-flight calibration compensates for this response loss, and there is no impact to the science data products due to this effect.

C. Signal-to-Noise Ratio

For unaveraged data, the MISR instrument specifications on signal-to-noise (SNR) call for SNR > 700 at full scale (100% equivalent reflectance). The specification on 4×4 pixel-averaged data is band-dependent and no less than 250 at an equivalent reflectance of 15%. During ARPgen processing, the SNR is determined from the unaveraged (1×1) data views of the diffuse panel. To measure SNR at a particular incident illumination level the in-band signal is determined from:

$$Signal_{in-band} = [\mathrm{DN} - \mathrm{DN_0}] * L_{in-band}/L_{total-band}. \quad (4)$$

The constant $L_{in-band}/L_{total-band}$ is the in-band to total-band ratio, and has been determined preflight to be 0.98, 0.97, 0.97, and 0.98 for the four MISR bands. In this algorithm the signal is interpreted as that due to the radiance that falls within the in-band wavelength limits. Local data residuals are used to determine noise.

The SNR model has been described in [2]. This model includes contributions from photon, electronic, and quantization noise sources. As Fig. 8 shows, the measured SNR meets the instrument specification, and compares well with the predicted values.

D. Detector Uniformity of Response

MISR data are typically acquired in Global Mode, where data from 24 of the data channels are averaged to 1.1-km resolution prior to transmission from the spacecraft. Ideally, the flight computer would have knowledge of the gain response for each pixel, compute the radiance measured by each pixel, and then average these values before transmission. In practice, an error is incurred by the process of transmitting the average DN value, then later during the ground processing converting to radiance using instrument gain coefficients averaged over 4×4 pixel blocks. The error is greatest for pixel subsets where the nonuniformity of response is large (within a 4×4 pixel block) and where the scene is inhomogeneous over a 1.1-km cross-track distance.

The Detector Data Quality Indicator (DDQI) reported within Level 1B1 data is a function of the detector properties alone. It is a simplified metric that discloses what radiometric error may be incurred due to nonuniformity of detector response. Scene uniformity is not considered in reporting this metric. (The
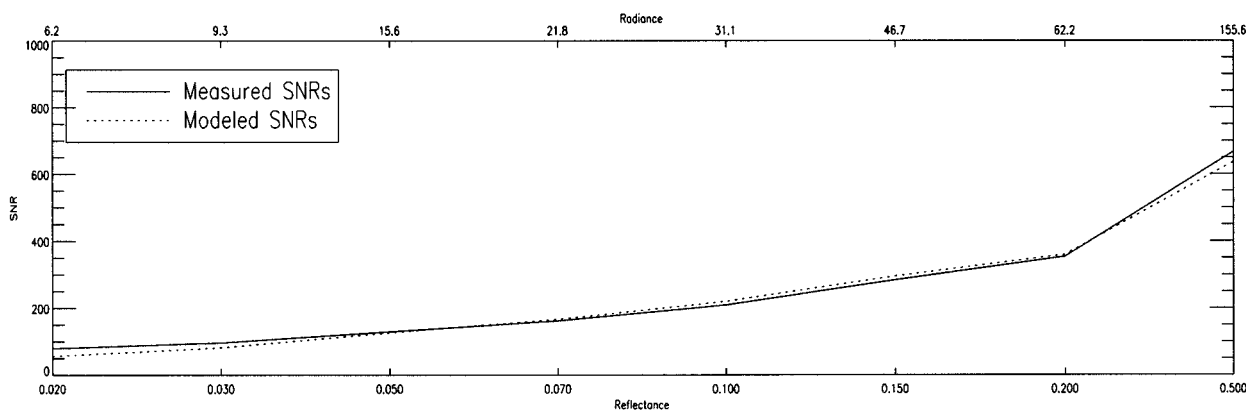
Fig. 8.   Measured versus predicted SNR for the An camera, Red Band.

TABLE IX
DDQI CRITERIA

DDQI value	SNR criteria at full scale	LNUR criteria	Radiometric quality of data product
0	SNR > 100	LNUR < 10%	Within specification
1	90 < SNR ≤ 100	10% ≤ LNUR < 15%	Reduced accuracy
2	10 < SNR ≤ 90	15% ≤ LNUR ≤ 50%	Questionable accuracy for certain scientific applications
3	SNR ≤ 10	LNUR > 50	Not usable for scientific applications

TABLE X
PIXEL BLOCKS WITH NONZERO DDQI FOR 4 × 4 DATA MODE

Camera	Band 1/ Blue	Band 2/ Green	Band 3/ Red	Band 4/ NIR
Df	75	375	375	
Cf				283
Bf				354, 355
Af		217*, 218		
An				
Aa		0	95	
Ba		0		3
Ca				
Da				109*

* DDQI=2 for these pixels, else DDQI=1

Level 1B2 data quality indicator, called the Radiometric Data Quality Indicator (RDQI), makes use of weighted averages of these DDQI values, but again does not consider scene uniformity.)

Selecting from the larger result of two criteria, listed in Table IX, defines the $DDQI_{4\times4}$ parameters. The first criterion uses the 1×1 SNR values; the second makes use of the local nonuniformity of response parameter, LNUR. The LNUR parameter is computed as the largest deviation from the background response for any detector within a 4×4 pixel block. (The background response is determined by interpolation across pixels of anomalous response.)

From ARPgen output, we note that the DDQI values have not changed between first light (instrument cover open) and the present time period. Only 12 pixel sub-blocks have nonzero DDQI values. (Two of these will never be encountered in the data, as Global Mode data uses high-resolution data for the Red Band). These pixel blocks are listed in Table X. Two of these blocks have been assigned a DDQI of 2, due to the LNUR criteria. The remaining pixel-blocks have DDQI = 1. To see the potential radiometric error, let us consider the worst case Cf, NIR value. For this pixel grouping the average SNR is 490, and the local nonuniformity of response is an 11.3% deviation from the background response. Consider an ocean scene, with a 275-m cloud centered over the least responsive detector field-of-view. Let the relative top-of-atmosphere relative radiances be 0.1 and 1.0, respectively. The error in the reported Level 1B1 can be computed as follows. The actual average radiance incident on the detectors is 0.325. The DN output for each pixel is approximated by the $G_1{}^*L$ product for that pixel, or 1*0.1, 1*0.1, 0.887*1, and 1*0.1, respectively. The average DN is 0.297, the average gain is 0.972, and the reported average radiance is 0.305. This gives a radiometric error of 6% for this extreme case. Note there would have been a 2% radiometric error had the cloud been in the field-of-view of a typical detector. Clearly this extreme scene contrast is rare, but the potential for error is flagged by setting the DDQI value equal to 2 for this case.

The Level 1B1 data product reports the computed radiance where the DDQI value does not equal 3, rather than replace the value with a fill value. It is recommended that other software packages, which make use of the radiances and DDQI values, also do the same.

Dark current is additionally monitored during the calibration experiments. Its magnitude is within one DN of the overclock readings. The dark current of the MISR cameras has not increased since launch.

E. Linearity

Discussed here are the radiometric errors attributed to the choice of calibration equation used to relate offset-subtracted digital numbers to radiance at the sensor. Several functional forms were evaluated against an arbitrary criterion. The goal is to have the reflectance error (due to the choice of calibration equation) be less than the larger of 0.001, or 0.01 times the reflectance. This criterion is plotted as the dashed lines of Fig. 9. The equations studied included a linear equation with no offset ($G_0 = 0$), a quadratic with no offset, and a power law where the DN is proportional to $G_1 L^{G2}$. To generate the curves shown in
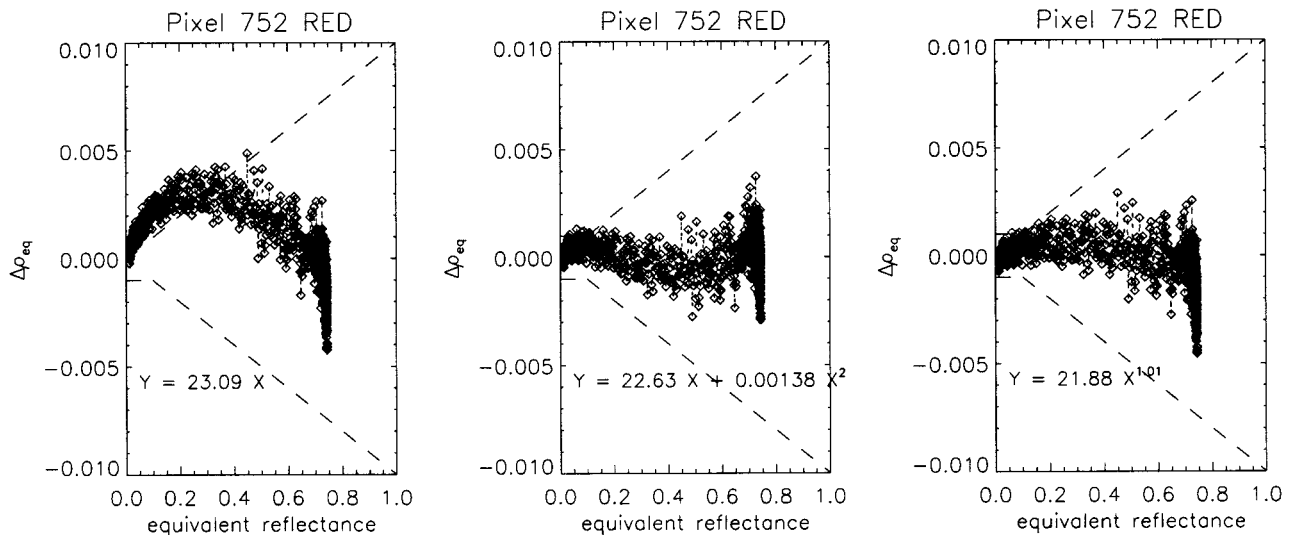
Fig. 9.   Reflectance error due to choice of linear, quadratic, or power-law calibration equations. Data used in this study came from the Bf camera, orbit 5361, but results are typical of the sensor response for all cameras and orbits.

Fig. 9, the camera DN versus incident radiance data, acquired for a given OBC calibration experiment, were processed assuming one of the candidate calibration equations. The residuals of measured DN, as compared to the DN predicted by the equation, are computed. These residuals are plotted expressed as a change in top-of-atmosphere reflectance, versus the incident radiance, expressed as an equivalent reflectance.

The result of this investigation concluded that the quadratic and power laws improved the radiance retrieval accuracy, as judged by a residual analysis for a given fit. The improvement is particularly good at low incident radiance values. As the improvement in accuracy between the quadratic and power law was minimal, the quadratic was selected as the functional form for the MISR cameras. This form had been selected preflight as the basis for the Level 1B1 radiance scaling code. The linear calibration equation that was implemented early in the mission, was replaced in the ARP T8_1 (May 17, 2001) time era, and continues to this date. It is also noted that should a particular camera or band channel be linear, the quadratic functional form would return a small quadratic coefficient during processing of the calibration data. Thus, this more complex calibration equation remains an appropriate descriptor even for a linear system.

V. SUMMARY

The success of the MISR in-flight calibration program is attributed to its on-board calibrator (OBC), which enables the camera-, band-, and pixel-relative calibrations. Paired with an annual vicarious calibration (VC) campaign, the OBC is also able to measure MISR absolute response changes on a bimonthly basis. The MISR cameras appear to be stable following initial on-orbit camera degradation. Updates to the coefficients used to scale camera DN output to radiance values render MISR science products insensitive to this slow instrument degradation. The in-flight calibration of MISR over the Nevada desert playa is believed to be accurate to within 4%. Comparing with MODIS, Landsat, and AirMISR radiance values has validated this.

Scene-dependent effects, such as point-spread-function (PSF) and ghost-image effects, are not accounted for in this Nevada site analysis. Therefore, the overall uncertainty of MISR is believed to be accurate to within 7%, with an additional 3% correctable bias resulting from within camera effects. These refinements will be the topic of future reports. It is anticipated that the present calibration approach will be maintained, even if scene-dependent corrections are made to future MISR data.

ACKNOWLEDGMENT

REFERENCES

[1] D. Diner, J. Beckert, T. Reilly, C. Bruegge, J. Conel, R. Kahn, J. Martonchik, T. Ackerman, R. Davies, S. Gerstl, H. Gordon, H. J-P., H. Muller, R. Myneni, R. Sellers, B. Pinty, and M. Verstraete, "Multi-angle Imaging SpectroRadiometer (MISR) description and experiment overview," *IEEE Trans. Geosci. Remote Sensing*, vol. 36, pp. 1072–1087, July 1998.

[2] C. Bruegge, V. Duval, N. Chrien, R. Korechoff, B. Gaitley, and E. Hochberg, "MISR prelaunch instrument calibration and characterization results," *IEEE Trans. Geosci. Remote Sensing*, vol. 36, pp. 1186–1198, July 1998.

[3] W. Abdou, C. Bruegge, M. Helmlinger, J. Conel, S. Pilorz, and B. Gaitley, "Vicarious calibration experiment in support of the Multi-angle Imaging SpectroRadiometer (MISR)," *IEEE Trans. Geosci. Remote Sensing*, vol. 40, pp. 1500–1511, July 2002.

[4] C. Bruegge, M. White, N. Chrien, E. Villegas, and V. Ford, "Multi-angle Imaging SpectroRadiometer (MISR) design issues influenced by performance requirements," *Proc. SPIE, Sensor Systems for the Early Earth Observing System Platforms,*, vol. 1939, pp. 104–113, April 1993.

[5] P. Slater, "A review of some radiometric calibration problems and methods," in *Proc. Int. Colloq. Spectral Signatures of Objects in Remote Sensing*, Bordeaux, France, 1983.

[6] C. Bruegge, V. Duval, N. Chrien, and D. Diner, "Calibration Plans for the Multi-angle Imaging SpectroRadiometer (MISR)," *Metrologia*, vol. 30, no. 4, pp. 213–221, 1993.

[7] C. Bruegge, A. Stiegman, R. Rainen, and A. Springsteen, "Use of Spectralon as a diffuse reflectance standard for in-flight calibration of earth-orbiting sensors," *Opt. Eng.*, vol. 32, no. 4, pp. 805–814, 1993.

[8] N. Chrien, C. Bruegge, and R. Ando, "Multi-Angle Imaging Spectro-Radiometer (MISR) On-Board Calibrator (OBC) in-flight performance studies," *IEEE Trans. Geosci. Remote Sensing*, vol. 40, pp. 1493–1499, July 2002.

[9] C. Jorquera, C. Bruegge, and V. Duval, "Evaluation of high quantum efficiency silicon photodiodes for calibration in the 400 nm to 900 nm spectral region," *In Proc. SPIE, Infrared Technology XVIII*, vol. 1762, pp. 135–144, 1992.

[10] D. Diner, J. Beckert, B. Bothwell, and J. Rodriquez, "Performance of the MISR instrument during its first 20 months in earth orbit," *IEEE Trans. Geosci. Remote Sensing*, vol. 40, pp. 1449–1466, July 2002.

[11] R. Woodhouse, C. Bruegge, B. Gaitley, G. Saghri, and N. Chrien, "Multi-angle Imaging SpectroRadiometer (MISR) Ancillary Radiometric Product (ARP)," in *Proc. SPIE, Earth Observing System II*, vol. 3117, July 1997.

[12] C. Bruegge, N. Chrien, and D. Haner, "A Spectralon BRF data base for MISR calibration applications," *Remote Sens. Environ.*, vol. 76, pp. 354–366, 2001.

[13] D. J. Diner, L. M. Barge, C. J. Bruegge, T. G. Chrien, J. E. Conel, M. L. Eastwood, J. D. Garcia, M. A. Hernandez, C. G. Kurzweil, W. C. Ledeboer, N. D. Pignatano, C. M. Sarture, and B. G. Smith, "The Airborne Multi- angle SpectroRadiometer (AirMISR): Instrument description and first results," *IEEE Trans. Geosci. Remote Sensing*, vol. 36, pp. 1339–1349, July 1998.

[14] C. Bruegge, M. Helmlinger, J. Conel, B. Gaitley, and W. Abdou, "PARABOLA III: A sphere-scanning radiometer for field determination of surface anisotropic reflectance functions," *Remote Sens. Rev.*, vol. 19, pp. 75–94, 2000.

[15] E. Early, P. Barnes, B. Johnson, J. Butler, C. Bruegge, S. Biggar, P. Spyak, and M. Pavlov, "Bidirectional reflectance round-robin in support of the earth observing system program," *Amer. Meteorol. Soc.*, pp. 1077–1091, Aug. 2000.

[16] World Climate Research Programme (WCRP) Publication Series 7, WMO ITD-no. 149, pp. 119–126, October 1986. The data was compiled by Christoph Wehrli, World Radiation Center (NRC), Davos-Dorf, Switzerland under WRC Publication 615, July 1985.

[17] *Solar Phys.*, 1997, vol. 171, pp. 283–302.

Nadine L. Chrien received the B.S. degree in engineering in the field of systems science from the School of Engineering and Applied Sciences, University of California, Los Angeles, and the M.S. degree in optical sciences from the University of Arizona, Tucson.

She is currently with the Jet Propulsion Laboratory (JPL), Pasadena, CA, as a System Analyst for MISR and is currently working as part of the MISR In-Flight Radiometric Calibration and Characterization team on algorithm development. Prior to her work on MISR, she worked on the Mars Observer Pressure Modulator Infrared Radiometer (PMIRR) alignment, target simulator, and calibration monochromator systems.

Robert R. Ando received the B.S. degree in mechanical engineering from Duke University, Durham, NC, in 1973 and the M.S. degree in oceanography from Scripps Institution of Oceanography, La Jolla, CA, in 1978.

He has been with the Jet Propulsion Laboratory, Pasadena, CA, since 1996, providing software integration and test support and validating the radiometric calibration for the Multi-angle Imaging SpectroRadiomter (MISR) instrument

David J. Diner (A'01) received the B.S. degree in physics (with honors) from the State University of New York at Stony Brook in 1973 and the M.S. and Ph.D. degrees in planetary science from the California Institute of Technology, Pasadena, in 1977 and 1978, respectively.

He has been with the Jet Propulsion Laboratory, Pasadena, since 1981. He is currently a Principal Member of the Technical Staff and Leader of the Multi-angle Imaging Science Element in the Earth and Space Sciences Division. He has been involved in numerous NASA planetary and Earth remote-sensing investigations, and is Principal Investigator of the MISR experiment and its airborne counterpart, AirMISR.

Dr. Diner is a member of the American Geophysical Union and the IEEE Geoscience and Remote Sensing Society.

Carol J. Bruegge received the B.A. and M.S. degrees in applied physics from the University of California, San Diego, in 1978 and the M.S. and Ph.D. degrees in optical sciences from the University of Arizona, Tucson, in 1985.

Currently, she is a Co-Investigator on the Multi-angle Imaging Spectroradiometer (MISR) project and serves as the Calibration Scientist for that NASA Earth Observing System (EOS) instrument. Her experience is principally in the area of terrestrial remote sensing, calibration of remote sensing sensors, radiative transfer, and use of ground-truth measurements for validation and calibration of airborne and on-orbit sensors. She has been with the Jet Propulsion Laboratory, California Institute of Technology, Pasadena, CA, since 1985 and has been involved with the absolute radiometric calibration of the Landsat Thematic Mapper, AirMISR, and Airborne Visible and Infrared Imaging Spectrometer (AVIRIS) sensors. She has also provided for the flight qualification of Spectralon, a diffuse material now used on-orbit for the radiometric calibration of sensors. Previously, she has been a Principal Investigator in the First International Land Surface Climatology Program Field Experiment (FIFE), a NASA ground-truth experiment.

Wedad A. Abdou received the B.S. degree in physics and mathematics from Alexandria University, Alexandria, Egypt, the Diploma of Imperial College (D.I.C.) in electrical engineering from the Imperial College, London, U.K., and the Ph.D. degree in physics from Exter University, Exeter, U.K.

She is currently a Member of the MISR validation and calibration team at the Jet Propulsion Laboratory (JPL), Pasadena, CA. She joined the faculty of the Physics Department and the Center for Atmospheric and Space Sciences at Utah State University (USU), Logan, from 1974 to 1984, to teach and do research, primarily in the area of ionospheric and thermospheric chemistry. She has worked at Globesat, Inc., a small satellite company that spun out of USU, from 1986 to 1991, and she has been a member of the Technical Staff at JPL since 1991.

Mark C. Helmlinger received the B.S. degree in physics from the California State Polytechnic University, Pomona, in 1991.

He is currently a Field Research Engineer at the Jet Propulsion Laboratory (JPL), Pasadena, CA, responsible for acquiring *in situ* measurements used to calibrate the Multiangle Imaging Spectroradiometer (MISR) and validating its surface and aerosol parameters. He is responsible for the functionality of JPL's Portable Apparatus for Rapid Acquisition of Bidirectional Observation of the Land and Atmosphere (PARABOLA) instrument, and he maintains a suite of instruments which include multiple sunphotometers and surface radiometers. He was also a Consultant for JPL in 1989. He has been involved in two to three major field campaigns each year, including the Safari 2000 campaign in southern Africa, The Boreal Ecosystem Atmosphere Study (BOREAS), and the First International Land Surface Climatology Program Field Experiment (FIFE).

Stuart H. Pilorz, photograph and biography not availble at the time of publication.

Kurtis J. Thome received the B.S. degree in meteorology from Texas A&M University, College Station, and the M.S. and Ph.D. degrees in atmospheric sciences from the University of Arizona, Tucson.

He is currently an Associate Professor of optical sciences at the University of Arizona and has served as member of the Landsat-7, ASTER, and MODIS science teams. His research interests include atmospheric remote sensing, radiative transfer, and sensor calibration and atmospheric correction.